Exploration on Nonaxisymmetric Flow Phenomenon in a Slinger Injector

Fang Wang*
Associate Professor
Aeroengine Numerical Simulation Research Center, School of Energy and Power Engineering, Beihang University, Beijing, China
Jiangxi Research Institute of Beihang University, Nanchang, China
Chengdu Innovation Research Institute on Aircraft Power of Beihang University, Pengzhou, China

Yu-Dong Wang, *Master of Engineering*; Xiang Gao, *Master of Engineering*; Yu-Long Ye, *Master of Engineering*; Rui Liu, *Master of Engineering*; Han Gao, *Master of Engineering*
Aeroengine Numerical Simulation Research Center, School of Energy and Power Engineering, Beihang University, Beijing, China

Jie Jin
Professor
Aeroengine Numerical Simulation Research Center, School of Energy and Power Engineering, Beihang University, Beijing, China
Jiangxi Research Institute of Beihang University, Nanchang, China
Chengdu Innovation Research Institute on Aircraft Power of Beihang University, Pengzhou, China

The slinger is an important configuration of an aeroengine combustion chamber. It is well matched to smaller gas turbines that are more sensitive to cost than larger and more sophisticated models. The slinger combustor is inherently low cost itself, by eliminating fuel injectors and much of the fuel tubing and manifolding and also reducing costs in the requirements of the main fuel pump by operating at fuel delta pressures significantly lower than conventional fuel systems. The slinger's inherent drawbacks of increased combustion liner surface area and less atomization are less of a concern in a lower temperature, lower cost small turbines. The slinger's internal flow is of great significance to fuel atomization. This paper conducts experiments and numerical simulations on the slinger fuel injector. Numerical analysis and high-speed photography of the fuel slinger were applied to investigate the film flow pattern inside the slinger and the liquid phase distribution inside the combustion chamber to predict the flow field in an aeroengine combustion chamber. The transient Reynolds-averaged Navier–Stokes method, the volume of fluid method, and the discrete phase method were adopted in the simulation, and a high-speed camera and the rotational rig were used to perform the experiments. The nonaxisymmetric flow was present in the slinger and the combustor space. In the simulation results, the total mass-flow rate varies with time. Each hole's mass-flow rate value in the slinger is also different at the same time. The Sauter mean diameter (SMD) difference for each injection orifice is relatively small compared with the SMD difference caused by a rotation rate. The spatial distribution of the spray is also uneven as shown in the result of different single discharge channels' mass-flow rates. The experimental photos confirmed the simulation outcomes. The general theoretical analysis was made that these nonaxisymmetric phenomena were driven by the combined action of centrifugal force, surface tension, and instability phenomenon.

Nomenclature

F	volume fraction value
t	time, s
x, y	coordinates, m
u, v	velocities, m/s
ν	kinematic viscosity of water, m^2/s
ρ	density of water, kg/m^3
σ	surface tension of water and the air, N/m^2
σ_{ls}	surface tension of water and the solid surface, N/m^2
σ_{sg}	surface tension of solid surface and the air, N/m^2

Subscript

i, j	components along with directions

Introduction

The fuel slinger configuration annular combustion chambers have a long history, first used by Turbomeca in 1946. The slinger combustor is inherently low cost itself, by eliminating fuel injectors and much of the fuel tubing and manifolding and also reducing costs in the requirements of the main fuel pump by operating at fuel delta pressures significantly lower than conventional fuel systems. The inherent lightweight of a slinger fuel system offers benefits to smaller turbines as well. The slinger's inherent drawbacks of increased combustion liner surface area and less atomization are less of a concern at a lower temperature, lower cost small turbines. Slingers are well matched to smaller, lower temperature gas turbines; it has been widely adopted in many applications such as helicopters, drones, and cruise missiles due to their combination of compact size, efficiency at high altitude, and low impact on engine cost due to low fuel supply pressure and simplicity of manufacturing. It also has the characteristics of eliminating traditional fuel injectors and preventing the fuel system from being exposed to compressor discharge temperature, inherently reducing the tendency to coke. An example of an engine cross section and its slinger combustor is shown in Figs. 1 and 2.

*Corresponding author; email: fwang@buaa.edu.cn.
Manuscript received September 2020; accepted February 2022.

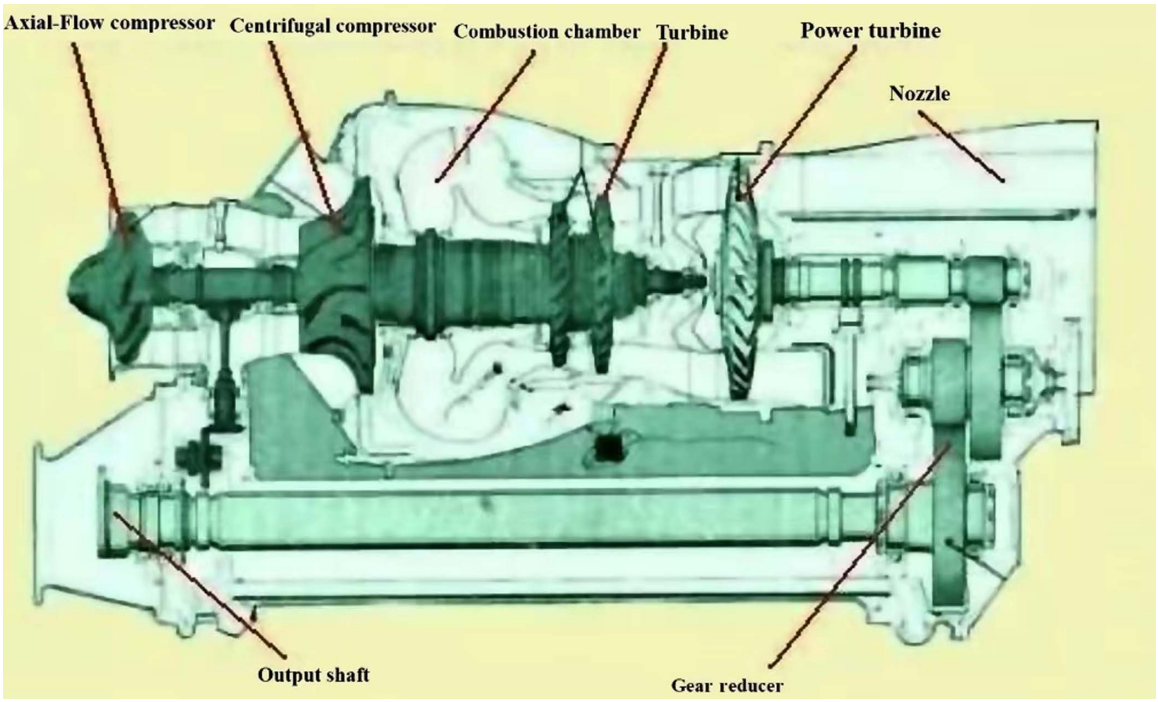

Fig. 1. Engine cross section.

In 1981, Morishita (Ref. 1) designed a new kind of fuel slinger for small-sized aeroengine. They formulated the empirical relationship between peripheral velocity and Sauter mean diameter (SMD) and found that it correlated with experimental data. Min et al. (Ref. 2) offered an experimental study on spray characteristics under atmospheric and pressurized cross-flow conditions, which is equivalent to the process of interaction between air and fuel after the fuel comes out of the slinger orifices. It was found that the spray profile is compressed, and the velocity distribution of fuel spray becomes more uniform when the ambient pressure is increased, as is found in the turbine engine combustion chamber. A deeper understanding of the primary breakup process was provided by Mazallon et al. (Ref. 3) in the form of a map with Weber's number as its x-axis and Ohnesorge's number as its y-axis to determine the way of primary breakup. Sallam et al. made the further observation (Ref. 4) in this regard to determine the breakup properties such as primary breakup regimes, conditions required for the onset of ligament, drop formation, and other parameters. A detailed study has been made by Desantes et al. (Ref. 5) to investigate the axis deflection and air entrainment of turbulent gas jets and diesel-like sprays in a crossflow. Scaling laws for the axis deflection of a jet/spray were obtained, and an original method to obtain fuel concentration along the axis of a jet/spray in a crossflow has been established by them. They have also found that there is a similarity in some ways when gas jets and diesel sprays interact with a crossflow. Sinha et al. (Ref. 6) studied experimental data on evaporation of droplets of decane, Jet-A1, and Jet-A1 surrogates using a spray-in crossflow configuration. They obtained evaporation constant k by iterative method and found out that there is a good match between the calculated droplet size distribution using the proposed k values and the measured one. It should be noted that studies mentioned above except Ref. 1 are written to study the breakup of nonturbulent round jets in gaseous crossflow, but they are highly similar thus relevant to the situation of the jets from the discharge channels. The information related to the flow in the slinger volume was offered by Werner et al. (Ref. 7) in the form of a formula to describe the thickness of the fuel film in the passages of the slinger. They have also given a method to correct the formulation when the Coriolis force is strong enough to influence the flow field. Different holes with different shapes and different rotation rates were also included in their study to investigate their effects on atomization. Some attempts were also made to reduce the empirical relations which have been suggested for determining the average droplet diameter to a unified system of parameters (Ref. 8). There were experiments to visualize the primary liquid breakup process, determine breakup lengths, and measure droplet sizes by varying rotational speed, liquid flow rate, injector hole shape, size and orientation, and the number of injection orifices (Ref. 9). Rezayat et al. (Ref. 10) extended the visualization study of the liquid breakup process in a slinger injector with high-aspect-ratio radial-axial discharge channels over a wide range of rotational speeds between 600 and 10,000 rpm to identify detailed breakup pattern and spray characteristics. Their research included images of the jet breakup and imaging analysis of particle/droplet to obtain the droplet-size distribution. A new phenomenon of jet bifurcation is also observed in their study.

Based on previous studies, the phenomena that the fluid film pattern in the passages of the slinger injector as well as the outflow injection will be studied by numerical simulation method and high-speed photography

Table 1. Simulation method of the film flow

Method Type	Method Adopted
Computational domain	The slinger volume and channels of the slinger injector
Mesh	Unstructured
Turbulence model	k–ε
Model for two-phase flow	Volume of fluid method
Boundary condition for the inlet	Mass flow inlet
Boundary condition for outlets	Pressure outlet
Boundary condition for the slinger walls	No-slip wall

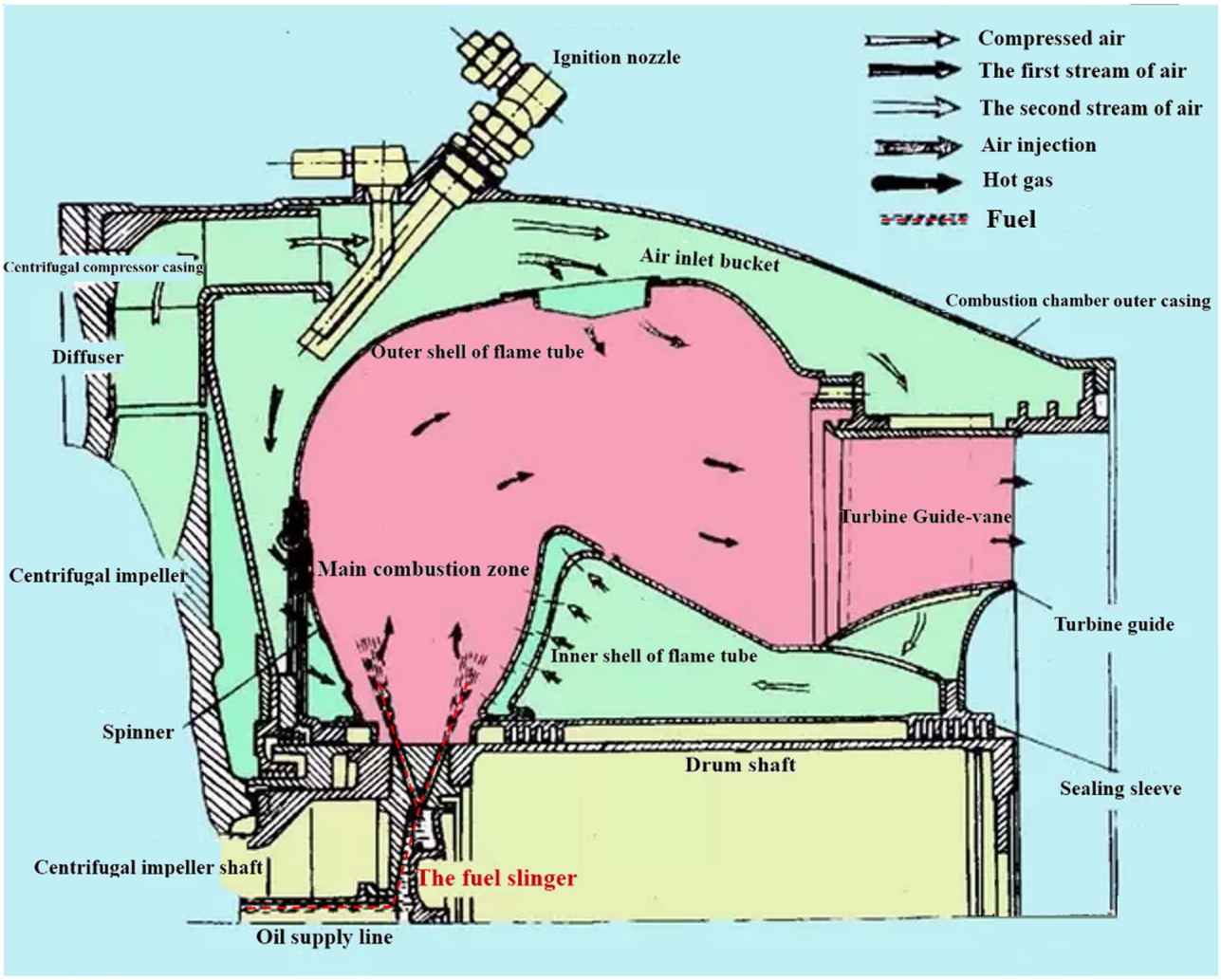

Fig. 2. Slinger combustor.

technology in this research, especially the instability both in time and space.

CFD Modeling

The commercial software ANSYS FLUENT was adopted to perform the simulation, which was divided into two parts for the flow in the slinger volume and the combustion chamber, respectively. For the second part, we simulate the jet that leaves a single orifice and the overall scene of liquid distribution in the combustion chamber. The fluid flowing through the slinger injector is set to be water. Both analyses used Reynolds-Averaged Navier–Stokes (RANS) as the governing equation, while different methodologies of liquid-air boundary tracking were taken as the majorities of fluid existing forms are film and droplets before and after the fluid leaves slinger holes. To be more specific, volume of fluid (VOF) and discrete phase method (DPM) were taken to treat in turn film flow and jet column breakup process.

Film-flow simulation

The water flow in the slinger volume is film flow as mentioned before. We treat it through transient simulation. The simulation method is shown in Table 1.

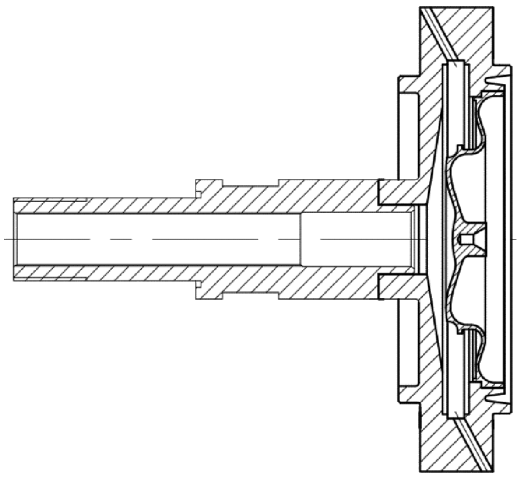

Fig. 3. Cross section of the slinger injector.

The computational domain for this part is the whole space inside the slinger atomizer, which is from a real engine with a maximum rotational rate of 22,000 rpm. Its configuration is shown in Figs. 3 and 4.

This slinger injector is made up of three key components, which are welded together. There are a fuel supply tube, a slinger pan, and a cover.

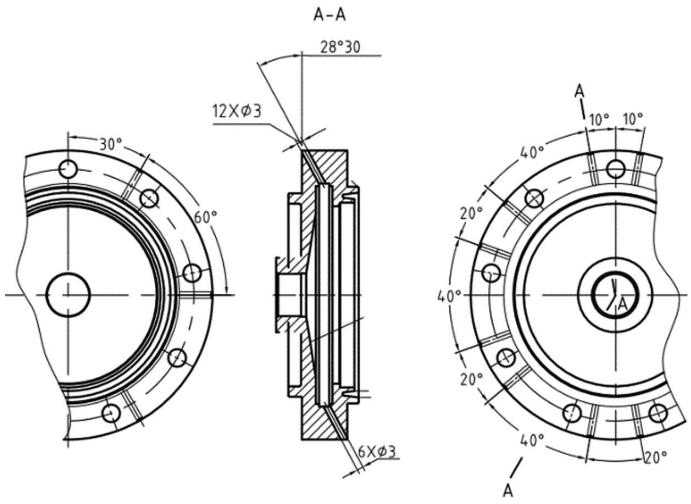

Fig. 4. Slinger holes' locations.

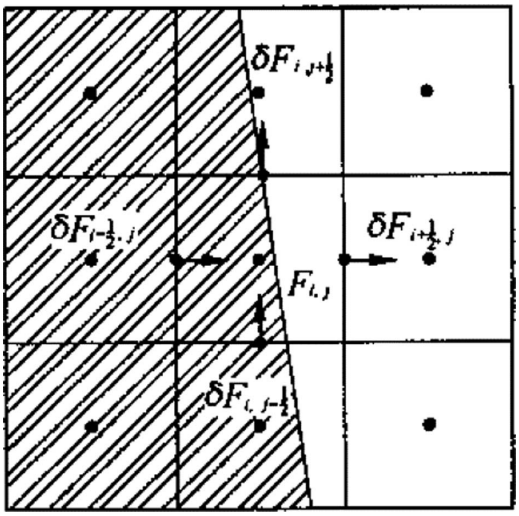

Fig. 5. VOF method.

The first part of the simulation used the chamber they form jointly as the computational domain. There are 18 orifices in total for this injector divided into two rows. The holes of the first row near the fuel supply tube are 20° or 40° apart from each other, while the second-row holes are set to be 60° apart.

The slinger injector is axisymmetric. Consequently, many previous studies like Refs. 7 and 9 used a slice of it to represent the integral film flow inside it or just performed experiments to investigate the jet column that comes out of one hole. This research simulates the entire slinger volume including the fuel supply tube and the small channels for the orifices to investigate local instability in fuel flow.

Experience showed that turbulence models of k–ϵ, Large-Eddy Simulation (LES), and Detached-Eddy Simulation (DES) (a mixed model from LES and RANS) can capture details of uneven two-phase flow in axisymmetric space (Ref. 11). The last two methods require far more computational resources than the first one. With limited CPU time and a computationally intensive task to calculate two-phase flow in the entire slinger volume transiently, k–ϵ was decided the most appropriate model.

Water is not completely filled in the slinger volume. There are liquid water and air in this slinger volume at the same time. Hence the Euler method VOF can fit to be the right two-phase flow model. This method tracks volume fractions for different phases to form the boundaries between these fluids. The volume fraction value is represented by F in this paper. If $F = 1$, the grid point is the place for a specific phase. If $F = 0$, the phase does not occupy the point. However, when F is somewhere between 0 and 1, it means that this kind of phase partially uses this control volume. The formulation to decide F and the figure to illustrate this method can be found as the following equation (Ref. 12):

$$F(x, y, z) = \begin{cases} 1, & \text{when this phase occupies } (x, y) \\ 0, & \text{when this phase doesn}'\text{t occupy } (x, y) \end{cases} \tag{1}$$

The transport equation for F in the conservative form can be written as

$$\frac{\partial F}{\partial t} + \frac{\partial uF}{\partial x} + \frac{\partial vF}{\partial y} = 0 \tag{2}$$

Using the grid shown in Fig. 5, which shaded the phase for F, we can get the first-order difference of (2) as

$$\frac{F_{i,j}^{n+1} - F_{i,j}^{n}}{\Delta t} + \frac{\delta F_{i+\frac{1}{2},j} - \delta F_{i-\frac{1}{2},j}}{\Delta x_i} + \frac{\delta F_{i,j+\frac{1}{2}} - \delta F_{i,j-\frac{1}{2}}}{\Delta y_i} = 0 \tag{3}$$

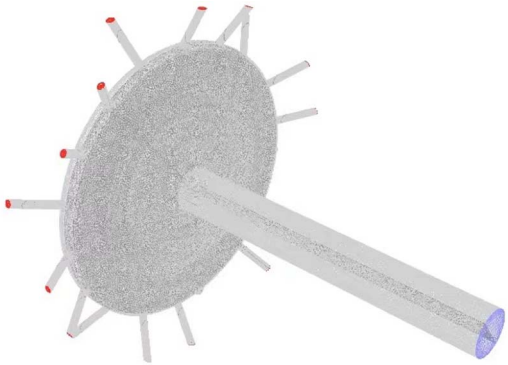

Fig. 6. Mesh to simulate the film flow in the slinger volume.

Table 2. Simulation method of the outer flow field

Method Type	Method Adopted
Computational domain	Space of the combustion chamber
Mesh	Structured
Turbulence model	k–ε
Model for two-phase flow	Discrete phase method
Boundary condition for the inlet	Velocity inlet
Boundary condition for the outlets of jets	Pressure atomizer
Boundary condition for the outlet	Velocity inlet
The boundary condition for the slinger walls	No-slip wall

Figure 6 illustrates the mesh used to simulate water flow in the slinger volume. The height of the first layer grid was 0.1 mm, small enough to ensure y^+ is around 50 which in turn guaranteed the validity of the k–ϵ turbulence model. The expansion ratio of the second layer against the first was 1.1 with the total cell number 4×10^6 .

The inlet of the fuel supply tube had the boundary condition of the mass-flow inlet in the simulation with the actual mass-flow rate for each rotation rate of the engine. The outlet was set to be a pressure outlet

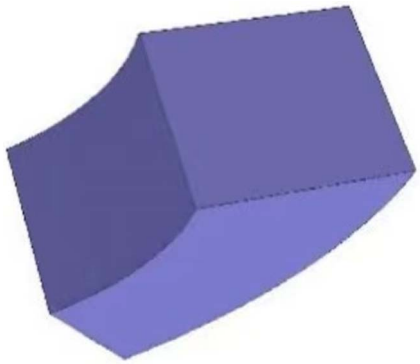

Fig. 7. The model to simulate one jet column's characteristics.

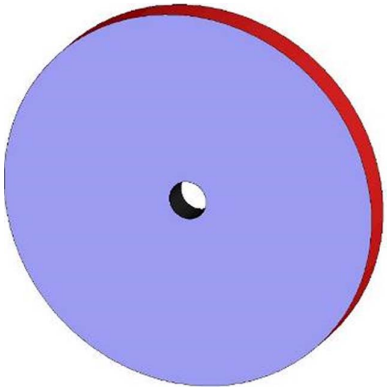

Fig. 8. The model to simulate the overall situation of all jet columns.

exposed to the atmosphere. The rest of the boundaries were walls that rotated with the whole slinger atomizer (see Table 2).

Jet-column breakup simulation

Different from the transient calculation of the film flow, semi-steady-state simulation with steady-state air environment and transient jet column and droplets computation (discrete phase method [DPM]) was in use.

Due to the nature of inclined orifices, the Coriolis force will make outcoming water a jet column (Ref. 7). Consequently, the single jet column can be simulated by using a pressure atomizer that is prebuilt with 0 atomizer dispersion angle and 0 spray half angle.

The space for this jet column to evolve in the cross-flow air and then break up is like a slice of cake without its tip as shown in Fig. 7. The inner radius is 70 mm, while the outer radius is 140 mm. The angle of this sector is 90° with a thickness of 60 mm. Under these parameters, the jet column will only leave the computational domain radially.

There is also another domain to simulate the overall situation of all 18 jet columns leaving those orifices. It is illustrated in Fig. 8. The outer radius is 700 mm, while the inner radius is the radius of the slinger injector with its thickness of 120 mm, significantly larger than the combustion chamber to allow us to know more about the detailed droplet distribution scene.

After the water leaves the holes, it can become fine fog full of small droplets with a diameter of microns (Ref. 13). Under that circumstance, many droplets can be considered as insignificant small disturbances with too small a volume compared to the whole grid cell, thus it will not be assessed by the model. As a result, the VOF method is no longer viable to calculate the jet breakup process in the combustion chamber.

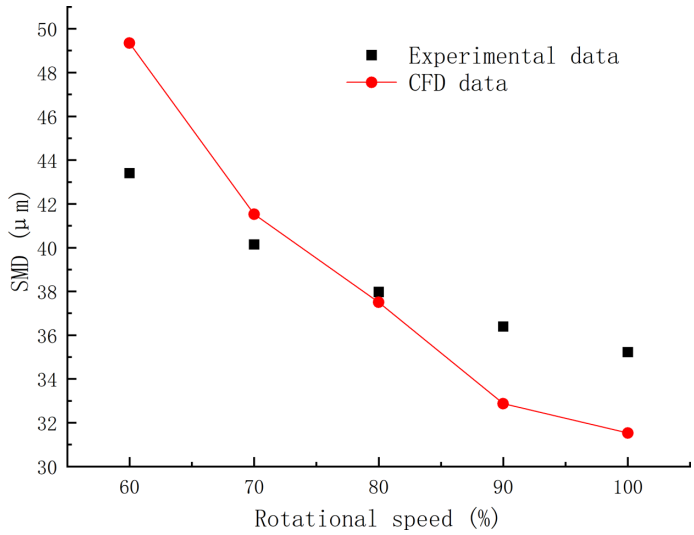

Fig. 9. Comparison of CFD data and experimental results (SMD) at each speed.

Table 3. Mass flow rates for different holes when the rotation rate is varied

Rotational Speed	Statistical Name	Out-Mass-Flow Rate (kg/s)	Difference to the Average Flow Rate (%)
60%	Maximum	6.72E−03	88.24
	Median	3.72E−03	4.20
	Average	3.57E−03	0.00
	Minimum	4.68E−04	86.89
70%	Maximum	7.60E−03	112.89
	Median	5.44E−03	52.38
	Average	3.57E−03	0.00
	Minimum	1.20E−03	66.39
80%	Maximum	2.35E−02	263.78
	Median	5.76E−03	10.84
	Average	6.46E−03	0.00
	Minimum	4.02E−03	37.77
90%	Maximum	1.91E−02	120.05
	Median	7.75E−03	10.71
	Average	8.68E−03	0.00
	Minimum	1.36E−04	98.43
100%	Maximum	2.00E−02	33.33
	Median	1.70E−02	13.33
	Average	1.50E−02	0.00
	Minimum	1.00E−02	33.33

Consequently, the DPM was adopted to solve the problem as it was used in a previous study and yielded great results (Refs. 14 and 15). And the turbulence model k–ϵ was taken based on the studies conducted before (Ref. 16), and it is also more computationally efficient.

The structured mesh was used for the analysis of water that came out of a single discharge channel with 1.02 million cells. The height of the first layer is 0.067 mm with an expansion ratio of 1.2 between the first and the second layer of the grid, insuring that y^+ is around 50, ensuring the validity. In contrast, the mesh of the whole space of the combustion chamber had 3.88 million structured grid cells but has the same first layer height and expansion ratio.

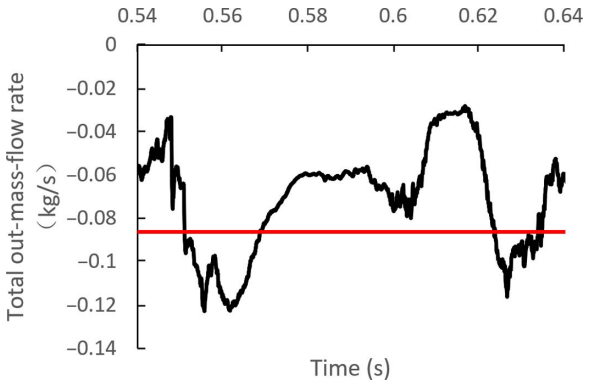

Fig. 10. The total out-flow-mass rate vs the time under 70% rotation rate.

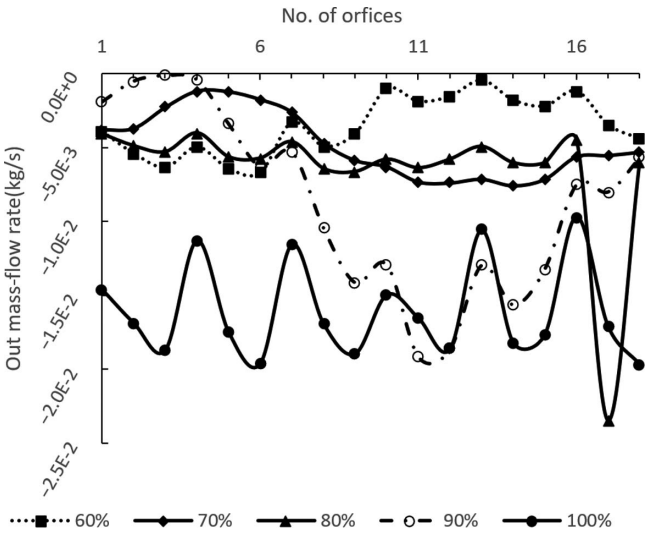

Fig. 11. The mass flow rates vs the hole's tag.

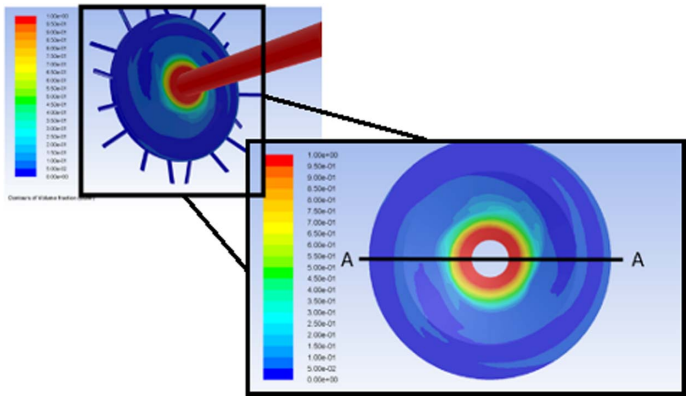

Fig. 12. Water film split up in the slinger volume.

The orifices were set to be pressure atomizers with 0 atomizer dispersion angle and 0 spray half angle. Except for the slinger walls, all the other boundaries were set as velocity inlets.

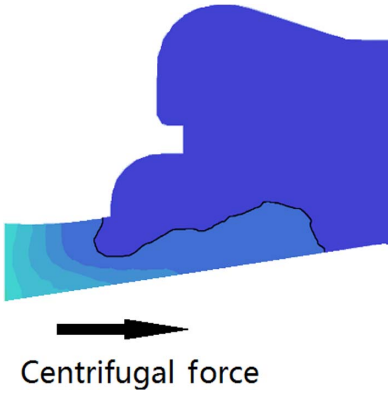

Fig. 13. A-A cross-section of Fig. 12.

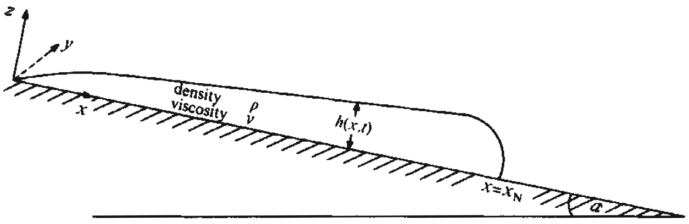

Fig. 14. Huppert's theory (Ref. 17).

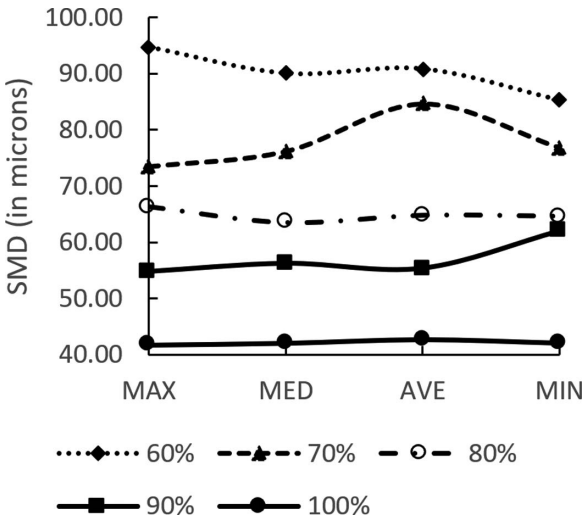

Fig. 15. SMD versus mass flow rates of the holes.

Simulation Results and Discussion

Numerical verification

Figure 9 compares the simulated SMD with experimental results at each speed. The experimental data were obtained by Phase Doppler Particle Analyzer (PDPA), and the experimental fuel slinger is consistent with the structure of this paper. It can be seen that the changing trend of the two is the same. At 60% speed, the relative error is the largest, which is 13.68%. Therefore, the numerical simulation in this paper is considered to be more reliable.

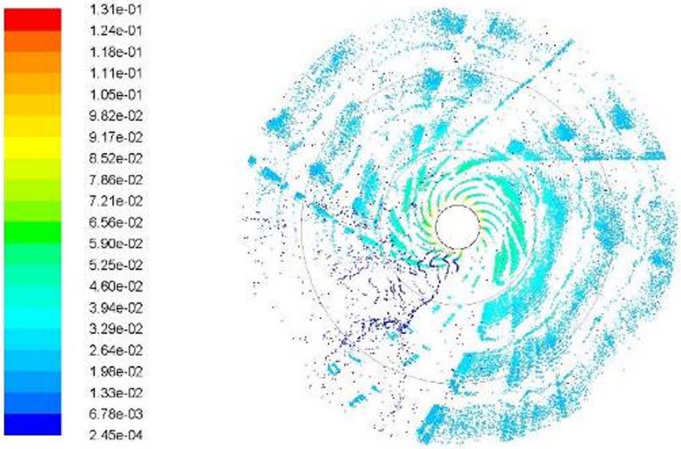

Fig. 16. "Real" droplet distribution.

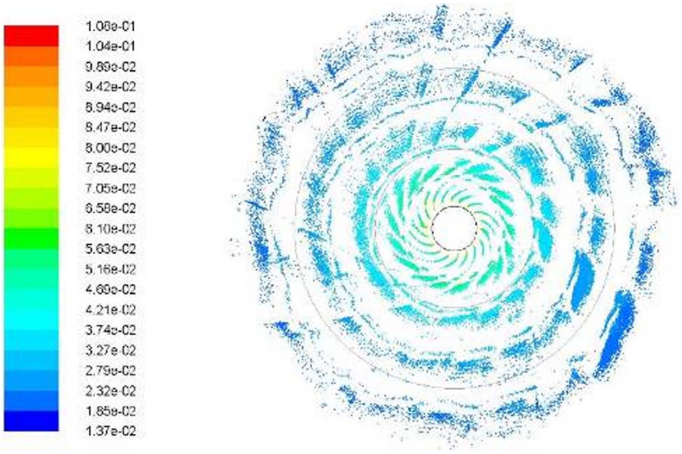

Fig. 17. Droplet distribution generated using a uniform orifice mass-flow rate.

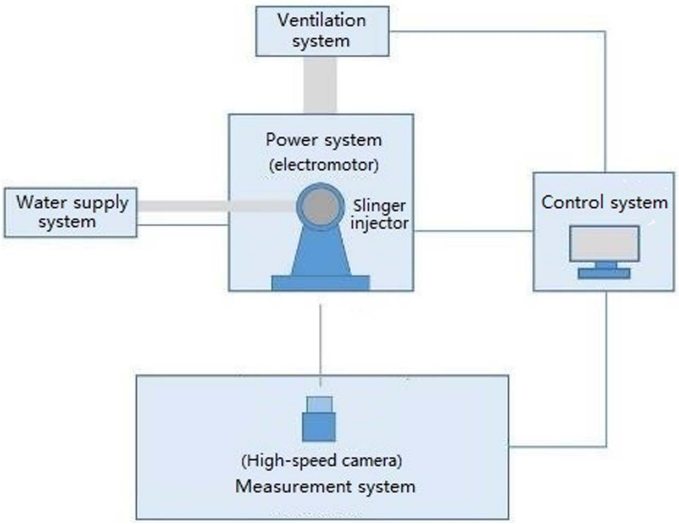

Fig. 18. The experimental rig.

Table 4. Details of the experimental facility

Parameter	Value
Experimental medium	Water
Medium temperature	Room temperature
Water supply pressure	0–0.6 MPa
Precision of flow valve	$\pm 2‰$
Total mass-flow rate	0–1200 L/h
Rotational speed of the slinger	0–22000 rpm
Maximum vibration	$\leq 1g$
Precision of the rotational rate	$\pm$ 100 rpm
Accelerating time	$\leq$10s (from 10,500 to 22,000 rpm)
Endurance	$\geq$1 h

Film flow

The relationship of out-mass-flow rate and the time is depicted in Fig. 10 when the rotation rate is 70% of the maximum it can reach. The red line represents the designed out-mass-flow rate with minus meaning the water comes out of the orifices. The figure shows that the total out-flow-mass rate is a function of the time as it varies much from the smallest number of 0.03 kg/s to the largest number of 0.122 kg/s. The difference of its peak and valley accounts for 75.4% of the total largest recorded out-flow rate and makes the total out-mass-flow rate highly related to the time.

The maximum, minimum, median, and average out-mass-flow rate of single holes as a function of the rotational speed are presented in Table 3. The difference to the average is gained by (4):

$$\text{Difference to the average} = \frac{|\text{The current flow rate} - \text{The average flow rate}|}{\text{The average flow rate}} \quad (4)$$

When the rotation rate is 80% of the maximum, the highest difference occurs as 263.78%. The minimum is 33%, while the most differences are around 100%.

Figure 11 gives us an idea of how the average outgoing mass-flow rate varies from one orifice to another during a period of 1 s and a picture of the influence from rotation rate to the mass-flow rate. It can be found out that under most rotational speed, several single discharge channels contributed to most of the total out-mass-flow rate. The mass flow concentrated in orifices numbers 1–9 as the rotation rate was 60% of the maximum while holes numbers 8–18 had the most water when the rotational speed was 70%. The most extreme scene occurred at 80% for most of the water flow through orifice number 17. Sinusoidal distribution of mass-flow rates appeared at the rotation rate of 100%. In conclusion, the assumption that the axisymmetric geometry of the slinger injector can lead to the axisymmetric distribution of outgoing water among orifices may not be valid based on the results of the simulation.

Coarse theoretical analysis of 2.2

The thickness of the water film is around 10 μm in the fuel slinger (Ref. 7), which falls into the situation described by Huppert (Ref. 17). In his paper, the water film flowing down a slope formed finger-like shapes due to instabilities, surface tension, and viscous force. Patches of dry areas can form downstream (Ref. 17) and exist stably as there is a balance of surface tensions σ_{ls} (surface tension of water and the solid surface), σ_{sg} (surface tension of solid surface and the air), and σ (surface tension of water and the air) (Ref. 18).

The centrifugal force acts like gravity described in Ref. 17 in the fuel slinger and leads to cylindrical coordinate 'finger shapes' shown in Fig. 12 (the redder the pixel is, the more water there is), which shapes the uneven distribution of mass-flow rate among orifices.

Table 5. Features of the high-speed camera

Parameter	Value
Maximum resolution	1280 × 1024
Maximum Frames Per Second (FPS) (@Resolution 1280 × 16)	62,000 frames per second
Maximum Frames Per Second (@maximum Resolution)	2550 frames per second
Operating temperature	−40 to 50°C
Sensor type	Complementary Metal-Oxide-Semiconductor (CMOS)
Sensor format	1 inch
Sensor size	13.9 × 11.1 mm
Pixel depth	10-bit mono/30-bit color
Pixel size (microns)	10.85 × 10.85 μm
Sensitivity	6000 ISO mono/2000 ISO color
Array	1.3 megapixel
Min. exposure time	1 μs
Image storage (@maximum frame rate)	4866
Quantum efficiency	60%
Sync-in	Phase-lock Through The Lens (TTL)
Sync-out	Frame sync/ strobe
Trigger	Through The Lens and switch/ circular buffer with on-camera or software trigger
Ethernet	100/1000 Base T
File formats	Raw
Software	Motion Studio/Inspector
On-the-fly conversion	tif, jpg, bmp, avi, png, mpg,

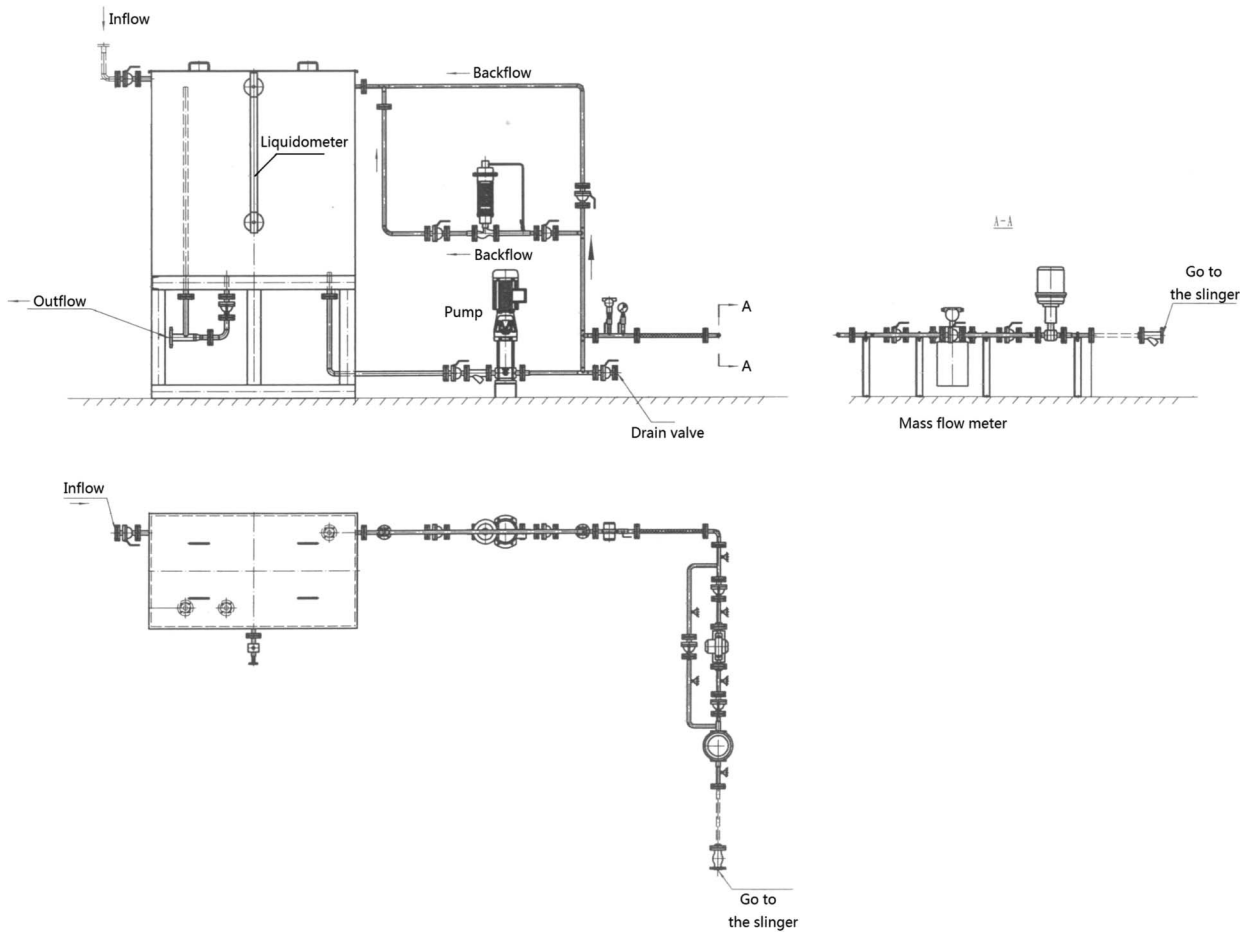

Fig. 19. Water supply system.

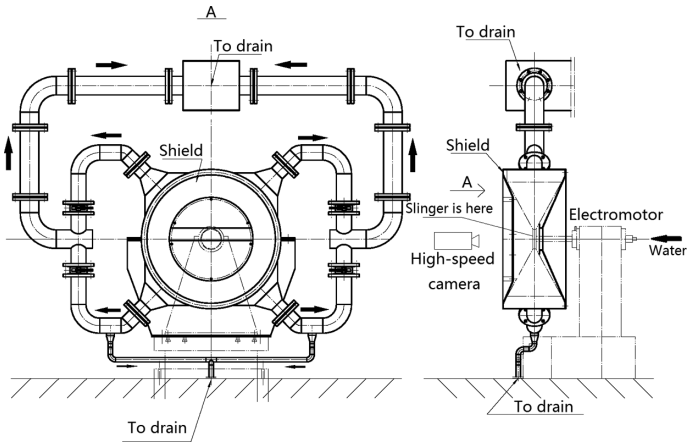

Fig. 20. Ventilation, power, and measurement system.

It can be observed from Fig. 13 the cross-sectional view of Fig. 12 that the profile of the water film front is just the same as Huppert described in Fig. 14 (Ref. 17). Consequently, Huppert's theory works in the volume of slinger injectors.

Single–orifice injection

Figure 15 illustrates the SMD distribution of a single discharge channel when the hole has different mass-flow rates under different rotation rates. The most noticeable feature is that the rotational speed is more influential than the mass-flow rates to the droplet size generated by the slinger. The mass-flow rates, however, still have some impacts on the SMD of a single orifice. Furthermore, droplet sizes can vary quite a lot as the slinger spins faster as there is a 100% difference in SMD between 60% and 100% rotational speed.

All-orifice injections

The outcomes were quite similar when the spinning speed was changed, so only one droplet distribution was picked to illustrate the overall scene. When the slinger was rotating as 90% as the fastest it can rotate, the "real" distribution of droplets in Fig. 16 is significantly more chaotic than what is produced by using the same mass-flow rates for all the holes in Fig. 17. Considering what is shown in 2.4, a conclusion can be reached that the uneven distribution of water flowing through different discharge channels can lead to a far less homogeneous spray field than what usually is expected thus causing deviation from the real combustion to the simulated combustion.

Experimental Setup

The main experiment system (see Table 4) consists of a measurement system (a high-speed camera; Table 5), an auxiliary system (a water supply system, a control system, and a ventilation system), and a power system (an electromotor and its accessories illustrated in Figs. 18–21. The rotating speed of the electromotor can be changed continuously under the control of a computer and the data can be recorded by the computer at the same time.

In the experiment, water is pumped from the water tank to the electromotor and then into the slinger injector. The control system can be utilized to change the rotational speed from 0 to 22,000 rpm continuously and to command the high-speed camera while the valve and the water pump can be used to adjust the total mass flow rate of the slinger. The fog generated by the slinger can be sucked out through ventilation tubes by a powerful fan in the ventilation system so that the jet column from the orifices can be seen clearly.

Experimental Results and Discussion

Figure 22 was taken under the rotational speed of 1000 rpm, total mass-flow rate of 935.8 kg/h, and Reynolds number of 2.1×10^4. It can be inferred from this photograph that the inner surface condition of the slinger volume was as intended, as the water jet distributed equally among slinger orifices with nothing blocking the holes.

The situation changed, however, when the rotational speed was set to 6000 rpm in Figs. 23 and 24, which illustrate the scene of different orifices in the same position. There was almost no water coming out of the lower hole in Fig. 23, while the jet column was quite strong when it came to the discharge channel in the same position in Fig. 24. These two pictures along with Fig. 22 provided qualitative proof to support the simulation outcome in 2.2 that the distribution of water among orifices is uneven.

Figure 25 has the same operating condition as Figs. 23 and 24 have but distinguish the difference of mass-flow rates through orifices more clearly

Fig. 21. The photograph of the experimental rig.

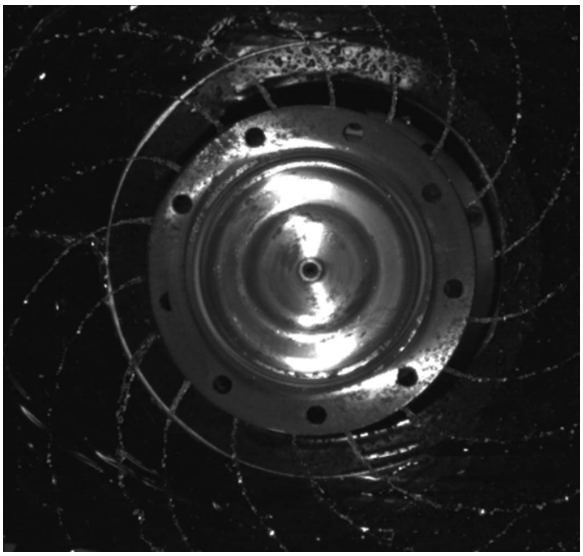

Fig. 22. The mass-flow rates are even under the low rotation rate.

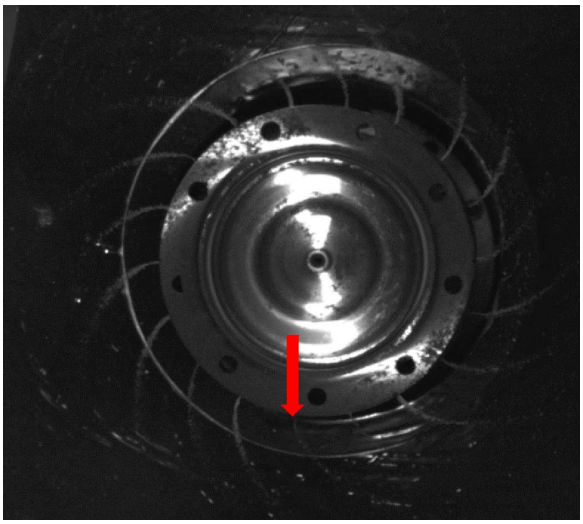

Fig. 23. The mass-flow rate of the hole in the lower hand position is almost 0.

with arrows marking the distinction of jets coming from neighboring holes. Only the lowest hand orifice has a white column.

Conclusions

Simulation and experiments were performed to study the film flow in the slinger volume. Transient computation was taken to simulate the film flow while the semitransient simulation was used to study the jet-column breakup and droplet distribution in the combustion chamber. Five main points could be gained through the experiments and simulation mentioned before:

1) The film flow is unstable with the variation of the total out-mass-flow rate. The difference can be as high as 75.4% of the average out-mass-flow rate.

2) The distinction between mass-flow rates of varied orifices can be 200% as the surface tension; the centrifugal force and instability phenomena can lead to a "finger-shaped" water film.

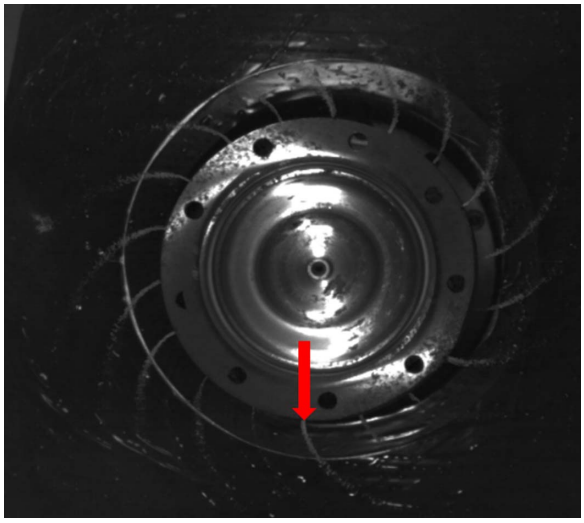

Fig. 24. The mass-flow rate of the hole in the lower-hand position is relatively large.

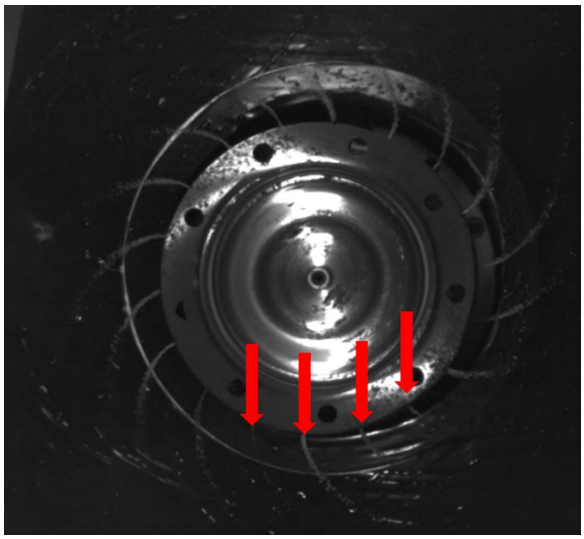

Fig. 25. Different holes with a different mass-flow rate in the same photograph.

3) Rotational speed is more influential to the SMD of each orifice than the mass-flow rate. There was a 100% difference in the droplet size described in SMD as the SMD of 100% rotational rate is around 42 μm, while the SMD of 60% rotational speed is 90 μm. The difference of SMD generated by the mass-flow rate is 11.17 μm when the rotational rate is 70%.

4) The spray field in the combustion chamber can be quite uneven as a result of the nonaxisymmetric distribution of the film flow in the slinger passages.

5) The experimental results from high-speed photography visibly supported the above conclusions.

Acknowledgments

This study was supported by the National Science and Technology Major Project (2017-I-0004-0005, 2017-I-0001-0001), and the National Natural Science Foundation of China (91741125).

References

[1]Morishita, T., "A Development of the Fuel Atomizing Device Utilizing High Rotational Speed," *ASME 1981 International Gas Turbine Conference and Products Show*, Houston, TX, March 9–12, 1981 American Society of Mechanical Engineers, New York, NY, 1981, V001T04A7.

[2]Min, G., Shimasaki, N., Nishida, K., Ogata, Y., and Wada, Y. J., "Experimental Study on Fuel Spray Characteristics under Atmospheric and Pressurized Cross-Flow Conditions," *Fuel*, Vol. 184, 2016, pp. 846–855.

[3]Mazallon, J., Dai, Z., and Faeth G. M., "Primary Breakup of Nonturbulent Round Liquid Jets in Gas Crossflows," *Atomization and Sprays*, Vol. 9, (3), 1999, pp. 291–312.

[4]Sallam, K., Aalburg, C., and Faeth G. M., "Breakup of Round Nonturbulent Liquid Jets in Gaseous Crossflow," *AIAA Journal*, Vol. 42, (12), 2004, pp. 2529–2540.

[5]Desantes, J. M., Arrègle, J., López, J. J., and García, J. M. J. F., "Turbulent Gas Jets and Diesel-Like Sprays in a Crossflow: A Study on Axis Deflection and Air Entrainment," *Fuel*, Vol. 85, (14–15), 2006, pp. 2120–2132.

[6]Sinha, A., Prakash, R. S., Mohan, A. M., and Ravikrishna, R. V., "Experimental Studies on Evaporation of Fuel Droplets under Forced Convection Using Spray in Crossflow Methodology," *Fuel*, Vol. 164, 2016, pp. 374–385.

[7] Werner, J. A. Dahm, Prashant, R. P., and Bryan, H. L., "Visualization and Fundamental Analysis of Liquid Atomization by Fuel Slingers in Small Gas Turbine Engines," Proceedings of 32nd AIAA Fluid Dynamics Conference and Exhibit 2002, St. Louis, MO, June 24–26, 2002.

[8]Baranaev, M. K., and Tenyakov, V. I., "Centrifugal Injector Droplet Size over a Wide Range of Dispersant Properties," *Fluid Dynamics*, Vol. 5, (3), 1970, pp. 492–499.

[9]Sescu, C., "Experimental and Computational Study on Liquid Atomization by Slinger Injector," Ph.D. Dissertation, University of Toledo, 2011.

[10]Rezayat, S., Farshchi, M., Karimi, H., and Kebriaee, A., "Spray Characterization of a Slinger Injector Using a High-Speed Imaging Technique," *Journal of Propulsion and Power,* Vol. 34, (2), 2017, pp. 469–481.

[11]Wardle, K. E., Allen, T. R., Anderson, M. H., and Swaney, R. E., "Free Surface Flow in the Mixing Zone of an Annular Centrifugal Contactor," *AIChE Journal*, Vol. 54, (1), 2008, pp. 74–85.

[12]Hirt, C. W., and Nichols, B. D. , "Volume of Fluid (VOF) Method for the Dynamics of Free Boundaries," *Journal of Computational Physics*, Vol. 39, (1), 1981, pp. 201–225.

[13]Rezayat, S., Farshchi, M., Karimi, H., and Kebriaee, A. J., "Spray Characterization of a Slinger Injector Using a High-Speed Imaging Technique," *Journal of Propulsion and Power*, Vol. 34, (3), 2017, pp. 1–13.

[14]Ruan, C., Fang, X., Huang, G., Ho, H., and Fei, X., "Atomization Performance Study of a Fuel Injector in IGC by Experimental and Numerical Investigation," *Procedia Engineering*, Vol. 99, 2015, pp. 939–947.

[15]Yakhot, V., Orszag, S., Thangam, S., Gatski T., and Speziale, C. Z., "Development of Turbulence Models for Shear Flows by a Double Expansion Technique," *Physics of Fluids A: Fluid Dynamics*, Vol. 4, (7), 1992, pp. 1510–1520.

[16]Shih, T.-H., Liou, W. W., Shabbir, A., Yang, Z., and Zhu, J., "A New k-Eddy Viscosity Model for High Reynolds Number Turbulent Flows," *Computers & Fluids*, Vol. 24, (3), 1995, pp. 227–238.

[17]Huppert, H. E., "Flow and Instability of a Viscous Current Down a Slope," *Nature*, Vol. 300, (5891), 1982, pp. 427–429.

[18]Ruckenstein, E., "On the Break-up of Thin Liquid Layers Flowing along a Surface," *International Journal of Heat and Mass Transfer,* Vol. 14, (1), 1971, pp. 165–169.